

**GREEN HYDROGEN PRODUCTION PLANTS VIA BIOGAS STEAM AND
AUTOTHERMAL REFORMING PROCESSES: ENERGY AND EXERGY
ANALYSES**

Mariagiovanna Minutillo^a, Alessandra Perna^b, Alessandro Sorce^c

^aDepartment of Engineering, University of Naples “Parthenope”, Naples, Italy

^bDepartment of Civil and Mechanical Engineering, University of Cassino and Southern Lazio,
Cassino, Italy

^cDepartment of Mechanical, Energy, Management and Transportation Engineering,
University of Genova, Genova, Italy

Abstract

The use of biogas to produce “green hydrogen” represents an interesting solution for assuring sustainability in the energy and mobility sectors with lower costs and a continuous production. In this study, two hydrogen production plants using biogas as primary source, are studied and compared by applying the energy and exergy analyses for both the overall plant and components. The plants are designed as polygeneration systems able to produce high-pressure hydrogen, heat, and electricity for self-sustaining the energy consumption for purification, compression, and storage of the produced hydrogen. In this sense, these plants are proposed as on-site hydrogen production plants for the development of novel refueling stations.

The two proposed plants differ for the hydrogen production process: i) a biogas-to-hydrogen plant through steam reforming, ii) a biogas-to-hydrogen plant through autothermal reforming.

The results of the study have highlighted that the steam reforming-based configuration allows for achieving the best performance in terms of hydrogen production energy-based efficiency (59.8%) and hydrogen production exergy-based efficiency (59.4%). Moreover, the steam reforming-based configuration represents the best solution also considering the co-production of heat and hydrogen (energy-based efficiency 73.5 and exergy-based efficiency 64.4%), while

the ATR-based layout, globally more exothermic, can be adopted when a larger local heat demand exists (energy-based efficiency 73.9 and exergy-based efficiency 54.8%).

Keywords: Biogas, green hydrogen, SOFC, reforming, exergy analysis, refueling stations

NOMENCLATURE

A/B	Air to Biogas ratio (mol/mol)
ATR	Autothermal Reforming Reactor
B2H	Biogas to Hydrogen
C	Compressor
CB	Catalytic burner
CHH	Combined hydrogen and heat
δirr	External exergy losses (%)
E_x	Exergy (kW)
EL	Electrolysis
ε_{CHH}	Combined hydrogen and heat exergy-based efficiency (%)
ε_{th}	Heat production exergy-based efficiency (%)
ε_{H_2}	Hydrogen production exergy-based efficiency (%)
HE	Heat Exchanger
HRF	Hydrogen recovery factor
I	Current (A)
Irr	Exergy destroy (kW)
IC	Ionic compressor
LHV	Low Heating Value (MJ/kg)
MR	Membrane Reactor

<i>OCV</i>	Open Circuit Voltage (V)
<i>O/C</i>	Oxidant to carbon ratio (mol/mol)
<i>Pd-M</i>	Palladium Membrane
<i>PSA</i>	Pressure swing adsorption
<i>S/C</i>	Steam to carbon ratio (mol/mol)
<i>S/B</i>	Steam to Biogas ratio (mol/mol)
<i>SEP</i>	Separation unit
<i>SR</i>	Steam Reforming
<i>V_{stack}</i>	Voltage (V)
<i>VPSA</i>	Vacuum Pressure Swing Adsorption
<i>W</i>	Electric power (kW)
<i>W_{rev}</i>	Reversible work (kW)
<i>WGSR</i>	Water Gas Shift Reactor
<i>Φ</i>	Energy stream (kJ)
<i>η_{CHH}</i>	Combined hydrogen and heat energy-based efficiency (%)
<i>η_{th}</i>	Heat production energy-based efficiency (%)
<i>η_{H2}</i>	Hydrogen production energy-based efficiency (%)

1. Background and scope

Hydrogen is considered a promising fuel able to satisfy the requirements of green and clean mobility. However, hydrogen can be retained completely sustainable if the needed energy for its production is supplied from renewable sources, generating the so-called “green hydrogen”.

A recent study, supported by the European FCH-JU (Fuel Cells and Hydrogen Joint Undertaking) on the “green hydrogen”, has analyzed, from an economic point of view, the possible pathways to produce hydrogen from renewable energy sources, founding that the less

expensive and promising way is the bio-hydrogen production by using biogas reforming processes [1] or other biological processes like those based on bacterial photosynthesis techniques [2].

In [1] a techno-economic assessment of two conventional technologies for hydrogen production from biogas, steam reforming or autothermal reforming, was performed. In both cases, the reforming reactor was followed by two temperature-staged water gas shift reactors and a pressure swing adsorption for hydrogen separation. For the considered systems, the maximum efficiency of 52% is obtained with the steam reforming system.

Yao et al. [3] studied, through a techno-economic analysis, the production of CO₂-neutral H₂ by using three technologies: the dual fluidized bed biomass steam gasification, the biogas steam reforming, and the alkaline electrolysis powered by renewable electricity. Their results highlighted that the electrolysis process has the highest H₂ conversion efficiency (about 66%) compared to the biogas steam reforming (47%) and the biomass steam gasification (38.9%).

Di Marcoberardino et al. [4] investigated the potentiality of the membrane reforming reactor technology for green hydrogen production from biogas. The proposed solution was compared with conventional technologies based on steam reforming and autothermal reforming integrated with a pressure swing adsorption (PSA) unit for hydrogen purification. Results showed that the adoption of a membrane reactor increases the system efficiency by more than 20% points compared to the conventional plants.

Thus, biogas-based hydrogen production systems represent an interesting solution for assuring its sustainability. Since the energy requirements for the hydrogen production and storage should be satisfied internally to the plants, polygeneration/multi-energy systems (designed to produce multiple energy vectors) can be the optimal solution for simplifying, under technical and economical points of view, the introduction of hydrogen in the market of the sustainable

mobility and, thus, for the transition to low-carbon future energy systems with higher overall efficiencies.

Several studies on multi-generation systems for the co-production of multiple energy outputs, available in the technical literature, use the exergy analysis for identifying the thermodynamic losses in the plants and for detecting the components where it is convenient to set in to improve the energy system behavior and overall performances.

Cruz et al. [5] proposed a bio-hydrogen energy system integrated with a combined cycle power plant and analyzed its performance through the exergy analysis. The hydrogen production section consists of a methane dry reforming unit, high and low temperature water gas shift reactors, and a pressure swing adsorption unit. The combined cycle satisfies the electricity and the steam requirements of the fuel processing unit. Results highlighted that the system has an exergy efficiency of 55%, with the methane dry reforming unit and the power generation unit arising as the main sources of irreversibility.

Abusoglu et al. [6] proposed and analyzed different technical models for the green hydrogen production from biogas-based electricity and sewage sludge. These technical models include low and high temperature water electrolysis, alkaline hydrogen sulfide electrolysis, and dark fermentation processes. The exergy efficiencies of the models were calculated, and results pointed out that the best efficiency (60.5%) was achieved for the model based on the dark fermentation of sewage sludge followed by the high temperature steam electrolysis process.

Cohce et al. [7] proposed the exergy analysis as a useful tool for understanding and improving the efficiency of a hydrogen production plant based on biomass (oil palm shell) gasification, steam methane reforming, and shifting processes. The exergy efficiency of the plant, simulated by using the Aspen Plus™ software, resulted equal to 19%.

A novel multi-generation system (heating, cooling, electricity, hydrogen, water) fed by biogas and geothermal heat source was proposed by Rostamzadeh et al. [8]. The authors applied the

first and second laws analyses as effective tools to assess the plant performances and used a single and multi-criteria optimizations approach for estimating their improvement. By applying the optimization approach the maximum exergy efficiency of 83.6% was achieved.

Dincer and Zamfirescu [9] evaluated the advantages of multi-generation energy systems powered by renewable energy and compared several options from energy and economic points of view. Results of their study underlined that the multi-generation can help to increase both the energy and exergy efficiencies, to reduce the costs and the environmental impact, and to increase the energy generation sustainability.

Ahmadi et al. [10] presented a study in which the thermodynamic analysis of a new multi-generation system with six outputs was performed. The plant, based on a biomass combustor, an Organic Rankine cycle (ORC), an absorption chiller, a proton exchange membrane electrolyzer to produce hydrogen, and a domestic water heater for hot water production was investigated by using the exergy analysis. A parametric study to evaluate the effects of several design parameters on the energy and exergy system efficiencies was also applied.

Bhattacharya et al. [11] performed the exergy analysis on an oxygen blown biomass gasification system devoted to the hydrogen production. The exergy destruction in each component and/or process as well as and the effects of the oxygen purity and the gasifier equivalence ratio on the exergy efficiency were studied and analyzed. Results highlighted that the highest overall exergy efficiency of the system was 67% and, as expected, the gasifier was found to have the largest exergy destruction in the plant.

Therefore, as it can be inferred from the above-discussed references, some studies focus on the energy or exergy analysis of biogas-based polygeneration systems for the co-production of hydrogen, electricity, and heat, none of them account for the analysis of the purification, compression and storage sections necessary to the exploitation of the hydrogen in the mobility

sector. Other studies cover this application, but without a polygeneration approach, relying on grid supply for the electric consumption of the plant.

The novelty of this study lies in the comprehensive energy and exergy analyses on biogas-based polygeneration systems designed for producing high-pressure hydrogen and for self-sustaining the electric energy requirements of novel on-site refueling stations for fuel cell electric vehicles. Thus, this paper aims to provide an original contribution for the optimal use of biogas for the development of on-site refuelling stations for green and sustainable hydrogen production and distribution.

2. Plant layouts description: sections and technologies

The polygeneration of hydrogen, heat, and electricity is proposed through the designing of two biogas-based plants that differ for the fuel reforming process. Thus, the proposed configurations are i) biogas-to-hydrogen plant based on the steam reforming process (B2H_SR); ii) biogas-to-hydrogen plant based on the autothermal reforming process (B2H_ATR).

Figure 1 shows the schematic architecture of the plants. The biogas is produced in an anaerobic digestion plant that, in this analysis, not considered within the plant site boundaries. The biogas, consisting of 60% CH₄ and 40% CO₂, corresponding to an LHV of 17.7 MJ/kg, is sent to the reforming section (SR or ATR) for the syngas production [12]. Then, the syngas is split up for feeding two sections: the SOFC power section and the hydrogen separation section based on the Pd-membrane technology. Finally, in both configurations, the hydrogen is compressed and stored at high pressure (820 bar).

The size and the operating conditions of the hydrogen compression and storage section are the same for both the plant configurations because the hydrogen production rate, equal to 100 kg/day, has been assumed as a design constraint.

The power unit, based on SOFC modules, is sized to supply the electric power required by the hydrogen separation and the hydrogen compression and storage sections as well as the auxiliaries.

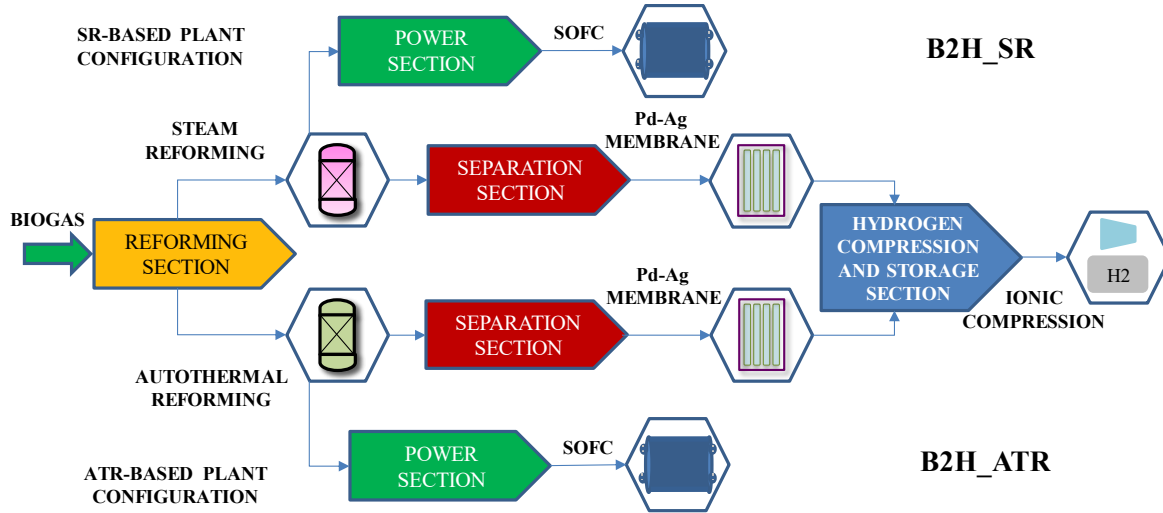


Figure 1. The B2H plant structure: the B2H_SR layout and the B2H_ATR layout

2.1 Description of the B2H_SR plant configuration

The B2H_SR plant layout is depicted in figure 2. In the steam reforming process, the biogas to be processed and the steam (the reforming agent) are sent to the SR reactor where the endothermic reforming reaction occurs in the presence of a catalyst. The required heat is supplied by an external source (usually a catalytic burner) and depends on the thermal balance of the reforming reactor where isothermal conditions are assumed. As widely reported in the scientific literature, the operating parameters controlling the hydrogen production are the reforming temperature and the steam to carbon ratio S/C [13]. High values of S/C allow increasing the hydrogen production and avoiding the carbon deposition on the reformer catalyst surface, but the heat required to sustain the steam reforming reaction also increases, with a negative effect on the overall system efficiency. This negative effect can be avoided by increasing the reactants' temperature by the thermal recovery of the internal hot streams. Moreover, in order to maximize the hydrogen production, a low-temperature step in which CO is converted to CO₂ via water gas shift reaction is needed.

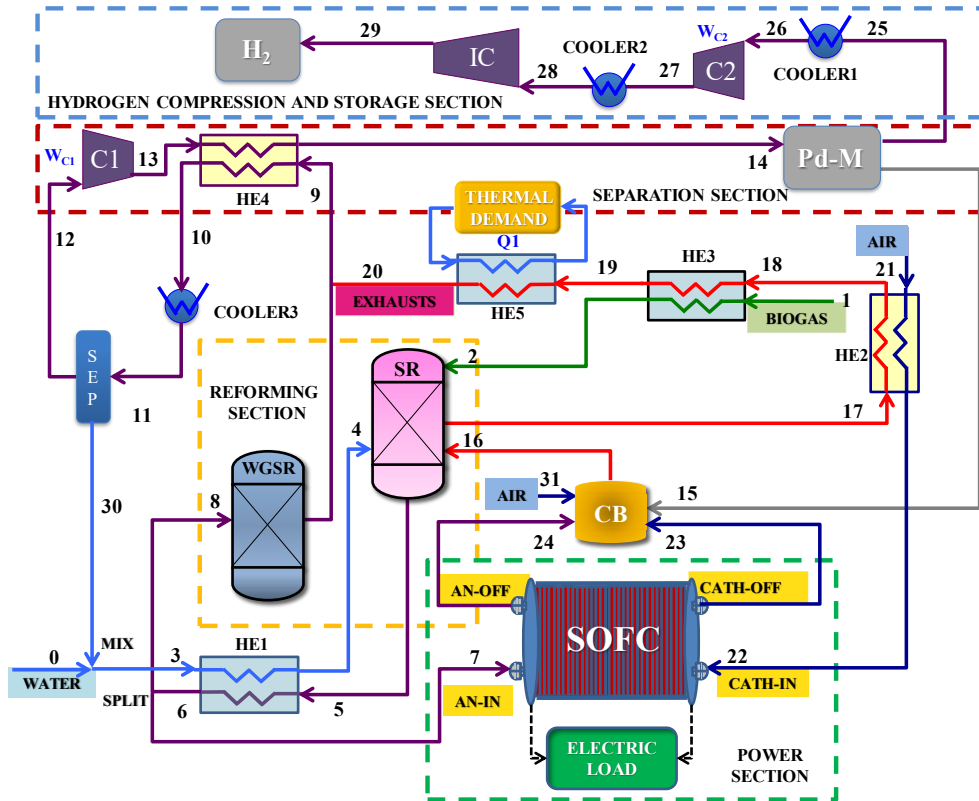


Figure 2. The B2H_SR plant configuration

Thus, the biogas (stream 1) is heated in the heat exchanger HE3 up to 300°C while water (3) is preheated, vaporized and superheated in HE1 till 300°C before entering the SR reactor. The syngas (5), produced at 767°C and consisting of a mixture of H₂, CO, CO₂, and H₂O, is cooled up to 326°C in HE1 and then is separated in two fluxes: the first one (8) is sent to the Water Gas Shift Reactor, WGSR, while the second one (7) feeds the SOFC power unit.

The required heat for the steam reforming reaction is supplied by the exhausts from the catalytic burner, CB. This component is fed with the SOFC exhausts (23 and 24), the purge gas (15) from the Pd-M membrane, and fresh air (31). The thermal recovery from the exhausts (17) exiting the SR reactor allows to heat up the biogas and the air to the SOFC cathode at 260°C in HE2; finally, the exhausts (19) are sent to the heat exchanger HE5 for producing useful heat, Q1 for cogeneration purpose.

In order to reach the operating conditions of the Pd-M membrane, the stream (9) is cooled in the heat exchanger HE4 and dried in the separator, SEP, before to be compressed in the

compressor C1 up to 4.6 bar (i.e. the membrane operating pressure in the feeding side); the syngas is heated up to 400°C in HE4 before entering the membrane (14). The pure hydrogen (25) is sent to the hydrogen compression and storage section where it is cooled by Cooler1 at 20 °C and pre-compressed at 5 bar by C2. Finally, the hydrogen (28) is cooled and compressed in IC (Ionic Compressor) up to 820 bar.

2.2 Description of the B2H_ATR plant configuration

Figure 3 shows the B2H_ATR plant configuration. The autothermal reforming process is a combination of the steam reforming and the partial oxidation processes in which the thermal energy required by the reforming reactions is internally provided by burning a portion of the processed fuel with air under sub-stoichiometric ratio. The main operating parameters of the process are the temperature, the steam to carbon ratio (S/C), and the oxidant to carbon ratio (O/C). The conversion of hydrocarbons is improved as the reforming temperature rises, as reported in [14,15], reaching values greater than 99% in the range of 700-800 °C.

Thus, the temperature of 767°C has been selected. Moreover, as suggested in the literature concerning the biogas reforming processes, the S/C ratio has been assumed equal to 2 and, as a consequence, the amount of air at the inlet of the ATR has been calculated taking into account the need of balancing the heat required by the endothermic reforming reaction (steam reforming reaction) and maintaining the reactor at the selected operating temperature [16,17].

In order to have high thermal efficiencies (i.e. the ratio between the chemical energy of produced hydrogen and the chemical energy of the input fuel) a low-temperature water gas shift reaction step for the CO conversion into CO₂ and a thermal recovery of hot streams within the system are required. Thus, the reactants streams, biogas (1) and air (2), are heated in the heat exchangers HE3 and HE4 respectively up to 320°C and 580°C, while water (3) is pre-heated, vaporized and superheated in the heat exchanger HE1 till 550°C before entering the ATR reactor.

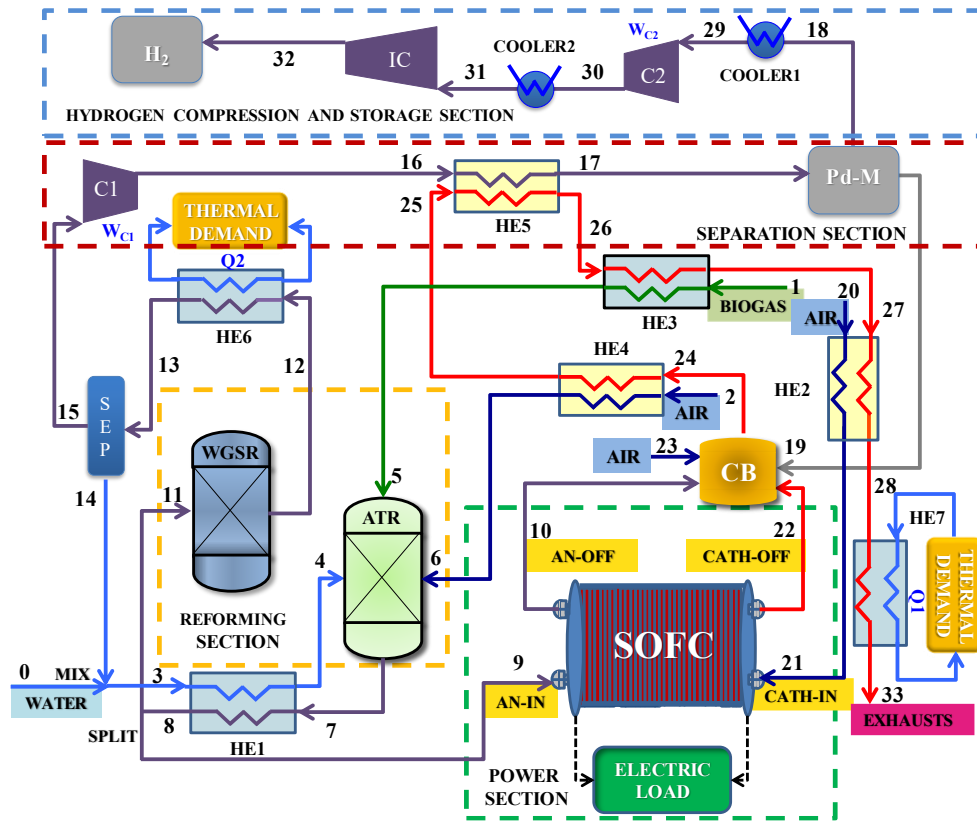


Figure 3. The B2H_ATR plant configuration

The syngas (7), consisting of H_2 , CO, CO_2 , H_2O , and N_2 , leaves the ATR reactor at $767^\circ C$ and is cooled down to $328^\circ C$ in the HE1 where the steam is generated. Then, as in the B2H_SR configuration, the syngas is separated in two fluxes that feed the WGSR (11) and the SOFC power unit (9). The air (20) for the cathode side of the SOFC is pre-heated at about $368^\circ C$ (21) in the heat exchanger HE2. The hydrogen-rich gas exiting the WGSR (12) is cooled in the heat exchanger HE6 and dried in the separator, SEP, before to be compressed in the compressor C1 at the feeding side operating pressure, 8 bar, of the membrane separation unit, Pd-M. Then, the compressed hydrogen-rich gas (16) is heated in HE5 to reach the operating conditions of the Pd-membrane, where the product hydrogen is recovered at 1.1 bar. Finally, in the hydrogen compression and storage section, the pure hydrogen (18) is cooled at $20^\circ C$ and pre-compressed at 5 bar in the compressor C2 (30) and sent to the ionic compression unit for reaching the storage pressure of 820 bar (32) after cooling in cooler2 (31). The purge gas (19)

coming from the membrane is oxidized in the catalytic burner, CB, together with the cathode off-gas (23), the anode off-gas (10), and the fresh air (33). The exhausts from the catalytic burner exchange heat with more streams (heat exchangers HE2, HE3, HE4, HE5, HE7), before being vent (28) at 156 °C. Thermal power (Q1 and Q2) for cogeneration purposes is generated in the heat exchangers HE6 and HE7.

3. The energy assessment: the plants operating data and performances

The operating data required to perform the energy analysis have been obtained by using numerical modeling. The thermo-electrochemical models, developed using the Aspen Plus™ software and applied to simulate the plant configurations, have been presented and widely discussed in a previous paper [18]. The Peng-Robinson cubic equation of state, that can accurately describe both the liquid and vapor phase for systems containing hydrocarbons and related compounds and for high H₂ content systems in a wide range of pressure and temperature, has been used for evaluating properties and characteristics of each material stream. The integrated models, realized by using operator blocks already existing in the Aspen Plus library or proper developed (user blocks), have allowed calculating mass flows, temperatures, pressures, chemical compositions, heat fluxes, and electric power consumptions or productions and, therefore, assessing the energy balance of the plant configurations. In Appendix A the flowsheets of the developed models and data concerning the calibration and validation procedures are described.

The results of the design and sizing activities are summarized in table 1, while the main characteristics of the plants streams are listed in tables 3 and 4 for the B2H_SR and B2H_ATR, respectively.

Table 1. Main operating parameters and characteristics of the plants sections

Plant Configuration	B2H_SR	B2H_ATR
REFORMING SECTION		
Reforming reactor temperature (°C)	767	767

WGS reactor temperature (°C)	419	405
S/C (S/B); O/C (A/B)	1.4 (0.82)	2 (1.7); 0.6 (1.2)
SEPARATION SECTION		
<i>Pd-Membrane Separation Unit</i>		
Hydrogen Recovery Factor, HRF	0.800	0.747
Feed/Permeate sides pressure (bar)	4.6/1.1	8.0/1.1
Operating Temperature (°C)	400	400
Modules Number/ Module Tubes Number	8/15	9/18
Tube area (m ²)	0.0385	0.0385
Total area (m ²)	4.7	6.5
<i>Compressor C1</i>		
Pressure ratio	4.6	8
Polytropic efficiency	0.75	0.75
Electric power (kW)	7.0	18.4
HYDROGEN COMPRESSION AND STORAGE SECTION		
<i>Compressor C2</i>		
Pressure ratio		5
Electric power (kW)		4.0
Polytropic efficiency		0.75
<i>Ionic compressor IC</i>		
Stage Pressure ratio		2.77
Electric Power (kW)		11.0
POWER SECTION		
SOFC power unit (kW) DC/AC	25/24	38/36.4
Stacks number/ Cells number x stack	3/42	4/52
Active cell area (cm ²)	500	500
Average stack voltage/Current density (V/A cm ⁻²)	0.793/0.5	0.725/0.5
Stacks Temperature (°C)	800	800
U _F	0.75	0.79

The composition of the syngas exiting the reforming reactor as well as its flow rate is very different in the two plant configurations because of the type of the reforming process (i.e. in the ATR the nitrogen in the reactant air dilutes the reformat product). The hydrogen concentration in the syngas, before entering the WGSR, results equal to 53.3% in the B2H_SR and 25.8% in the B2H_ATR, respectively, while, after the WGSR, it becomes equal to 61.3% and 32.7%, respectively. These different values impact on the operating pressure (4.6 bar vs. 8 bar), on the hydrogen recovery factor (0.800 vs 0.747) and on the total area (4.7 m² vs 6.5 m²) of the Pd-M membrane unit.

On the contrary, the hydrogen compression and storage section is the same for both configurations (the plant is designed for producing 100 kg/day of hydrogen) and its operating parameters are defined according to the characteristics of the ionic compressor manufactured by Linde, as described in [19].

The SOFC power unit has been sized for supplying the electrical powers required by the hydrogen separation (compressor C1), compression (compressor C2 and ionic compressor IC), and storage sections, that are equal to 24.0 kW and 36.4 kW in the B2H_SR and B2H_ATR, respectively. These different energy requirements are due to the greater electric power required by the compressor C1 in the B2H_ATR because of the higher syngas flow rate (152.1 kg/h vs. 55.3 kg/h) and membrane operating pressure. In order to define the SOFC power unit characteristics, the single cell described in ref. [18] has been used as the single element of the SOFC stack and its polarization curves, calculated at 800°C and under different feeding fuel composition, have been considered. Thus, by fixing the operating current density (0.5 A/cm²) and the cell area (500 cm²), the average cell stack voltage (in order to take into account the additional losses passing from a single cell to multi-cells stack, a stack loss factor has been introduced as described in ref. [19]) and the electric power of each cell have been evaluated. At the nominal current density of 0.5 A/cm², the average cell voltage for the SR-based configuration is greater than that for the ATR-based one (0.793 V vs. 0.725 V) thanks to the better syngas quality. By using these data, the number of cells per stack and the number of stacks that allow to satisfy the electric power requirements have been calculated. Therefore, the SOFC power unit consists of 3 stacks with 42 cells/stack and 4 stacks with 52 cells/stack in the B2H_SR and B2H_ATR, respectively.

Table 2. Properties of the main B2H_SR streams

Stream	Composition % vol	Mass flow kg/h	Temperature °C	Pressure bar
0	100 H ₂ O	21.7	20	1
1	40 CO ₂ , 60 CH ₄	47.3	20	1
5	13.3 H ₂ O, 53.3 H ₂ , 25.2 CO, 7.8 CO ₂ , 0.4 CH ₄	73.0	767	1
7	13.3 H ₂ O, 53.3 H ₂ , 25.2 CO, 7.8 CO ₂ , 0.4 CH ₄	13.7	326	1
8	13.3 H ₂ O, 53.3 H ₂ , 25.2 CO, 7.8 CO ₂ , 0.4 CH ₄	59.2	326	1
9	5.4 H ₂ O, 61.3 H ₂ , 17.3 CO, 15.6 CO ₂ , 0.4 CH ₄	59.2	419	1
12	0.3 H ₂ O, 64.5 H ₂ , 18.3 CO, 16.5 CO ₂ , 0.4 CH ₄	55.3	27	1
14	0.3 H ₂ O, 64.5 H ₂ , 18.3 CO, 16.5 CO ₂ , 0.4 CH ₄	55.3	400	4.6

15	0.6 H2O, 26.7 H2, 37.8 CO, 34.1 CO2, 0.8 CH4	51.1	400	1
20	7.9 H2O, 69.3 N2, 11.6 O2, 11.2 CO2	456.0	100	1
21	79 N2, 21 O2	75.2	20	1
23	89.1 N2 10.9 O2	65.8	800	1
24	53.3 H2O, 13.5 H2, 6.3 CO, 26.9 CO2	23.2	800	1
25	100 H2	4.2	400	1
28	100 H2	4.2	20	5
29	100 H2	4.2	65	820
30	100 H2O	3.9	27	1
31	79 N2, 21 O2	315.9	20	1

Table 3. Properties of the main B2H_ATR streams

Stream	Composition % vol	Mass flow kg/h	Temperature °C	Pressure bar
0	100 H2O	28.8	20	1
1	40 CO2, 60 CH4	70.0	20	1
2	79 N2, 21 O2	126.4	20	1
7	24.5 H2O, 25.8 H2, 9.8 CO, 11.4 CO2, 28.5 N2	251.3	767	1
9	24.5 H2O, 25.8 H2, 9.8 CO, 11.4 CO2, 28.5 N2	72.8	328	1
10	44.9 H2O, 5.4 H2, 2.1 CO, 19.1 CO2, 28.5 N2	88.6	800	1
11	24.5 H2O, 25.8 H2, 9.8 CO, 11.4 CO2, 28.5 N2	178.3	328	1
12	17.7 H2O, 32.7 H2, 2.9 CO, 18.2 CO2, 28.5 N2	178.3	405	1
14	100 H2O	26.1	58	1
15	1.1 H2O, 39.3 H2, 3.5 CO, 21.9 CO2, 34.2 N2	152.1	58	1
17	1.1 H2O, 39.3 H2, 3.5 CO, 21.9 CO2, 34.2 N2	152.1	400	8
18	100 H2	4.2	400	1
19	1.5 H2O, 14.4 H2, 4.9 CO 30.9 CO2, 48.3 N2	148.0	400	1
20	79 N2, 21 O2	120.0	20	1
22	89.7 N2, 10.3 O2	104.2	800	1
23	89.7 N2, 10.3 O2	245.2	20	1
31	100 H2	4.2	20	5
32	100 H2	4.2	69	820
33	12.9 H2O, 67.1 N2, 8.0 O2, 13.0 CO2	586.0	146	1

Table 4 lists the energy balance and the overall performance of the proposed plant configurations. The performance indexes based on the energy balance (hydrogen production energy-based efficiency, heat production energy-based efficiency, combined hydrogen and heat energy-based efficiency), are defined as the ratio between the output energy stream (hydrogen/heat) or their sum and the input energy stream (biogas):

$$\eta_{H2} = \frac{\Phi_{H2}}{\Phi_{biogas}} \quad (1)$$

$$\eta_{Heat} = \frac{\Phi_Q}{\Phi_{biogas}} \quad (2)$$

$$\eta_{CHH} = \frac{\Phi_{H_2} + \Phi_Q}{\Phi_{biogas}} \quad (3)$$

where Φ_{H_2} and Φ_{biogas} are calculated by referring to their low heating value (120 MJ/kg and 17.7 MJ/kg for hydrogen and biogas, respectively).

Table 4. Plants energy balance and performances

	B2H SR	B2H ATR
Chemical power (LHV,kW)		
Biogas	232.5	344.2
Hydrogen	139.0	139.0
Electric power (kW)		
Gross power (AC)	24.0	36.4
Compressors power consumption (C1, C2, IC)	22.0 (7.0,4.0,11.0)	33.4 (18.4,4.0,11.0)
Auxiliaries power consumption	2.0	3.0
Net power	-	-
Thermal power (kW)		
Thermal demand Q1	31.9	86.8
Thermal demand Q2	-	27.6
Efficiencies		
Hydrogen production energy-based efficiency (%)	59.8	40.4
Heat production energy-based efficiency (%)	13.7	33.6
Combined hydrogen and heat energy-based efficiency (%)	73.5	73.9

Results of the energy analysis show that, in the B2H_SR plant, the hydrogen production energy-based efficiency is higher of about 19 percentage points than that of the B2H_ATR. This is due to the better quality of the syngas produced in the reforming section that allows to reduce the plant energy consumption. It is worth noting that the power required by the compressor C1 to bring the syngas up to the operating pressure of the membrane separation unit is lower because of the smaller syngas flow rate and pressure ratio with respect to that of B2H_ATR plant. On the contrary, the combined hydrogen and heat energy-based efficiency is almost equal (73.5% vs. 73.9%) since the B2H_ATR configuration, thanks to the greater flow rates of the hot streams, makes available much more heat for thermal utilities.

The Exergy Analysis is then used to evaluate the main source of irreversibility that arises in the proposed layout.

4. The Exergy Analysis

Generally, the performances of energy conversion systems are evaluated through analysis criteria based on the first law of thermodynamics (i.e. the system energy balance that allows to evaluate performance indexes such as the thermal efficiency, the electric efficiency or the cold gas efficiency according to the type of energy outputs). However, several authors claim that the thermodynamic performance of any process in which energy is converted from one form to another cannot be correctly measured only on the basis of the first law considerations, but rather that the flows of energy in and out should be expressed in exergy terms [20]. The Exergy Analysis allows to determine magnitudes, location, and causes of irreversibility sources in the plants, also providing a more meaningful assessment of the plant individual component efficiency [21]. Thus, since the Exergy Analysis seems to be an appropriate technique to assess and rank the irreversibility sources in the processes [22], it can be a useful tool in the design, evaluation, optimization, and improvement of the energy conversion (thermal and chemical power plants) systems [21].

In this section, the Exergy Analysis is applied to evaluate the irreversibilities and the losses generated in the B2H_SR and B2H_ATR plant configurations, studied either as a whole either by considering the single plant components.

4.1 Exergy of material streams

By neglecting the kinetic and potential exergies, the total exergy of a multicomponent material stream m , characterized by T , p and x , that are temperature, pressure, and composition of the stream at its initial state, IS, is given by summing the physical exergy ($Ex_{phys,m}$) and the chemical exergy ($Ex_{chem,m}$):

$$Ex_m = Ex_{phys,m} + Ex_{chem,m} \quad (4)$$

The physical exergy is the work obtainable by taking the material stream, through a reversible process, from its initial state to the environmental state, ES characterized by the reference conditions T_0 and p_0 . It is defined as:

$$Ex_{Phys,m} = Ex_m^{IS} - Ex_m^{ES} = \sum_k \dot{n}_k [(h_k^{IS} - h_k^{ES}) - T_0(s_k^{IS} - s_k^{ES})] + \dot{n}_m \cdot RT_0 \ln \left(\frac{p}{p_0} \right) \quad (5)$$

In the above equation, k refers to a specific species in the material stream, \dot{n}_k , h_k and s_k are its mole flow, enthalpy, and entropy, respectively, R is the universal gas constant and \dot{n}_m is the total mole flow of the material stream. Enthalpy and entropy are calculated by using polynomial equations and assuming as reference conditions for the ES the standard ones (25°C and 1 bar) [23].

The chemical exergy is the maximum work that can be recovered when the material stream is brought from the environment state to the dead state, DS, by a process involving only heat transfer and material exchange with the environment [24]. Thus, in the DS the material stream is characterized by T_0 , p_0 , and x_0 . It is calculated as:

$$Ex_{chem,m} = \dot{n}_m \cdot \left[\sum_k x_k \bar{e}_{chem,k} + RT_0 \sum_k x_k \ln(x_k) \right] \quad (6)$$

where $\bar{e}_{chem,k}$ is the standard molar chemical exergy of the k -th species. The second term on the right side takes into account the effect of the gas mixing on the chemical exergy; it is always negative, so that the resulting exergy of the mixture is less than the sum of the chemical exergies of each species. The values of the chemical exergy are derived from ref. [24] and the different physical states (liquid and vapor) of the water have been also considered in the analysis.

4.2 Exergy balance of the system

Referring to the system and its control volume “G”, the exergy balance is:

$$Ex_{in,G} = Ex_{out,G} + \sum_i W_{rev,i} + \sum_i Ex_{lost,i} + Irr_G \quad (7)$$

In the above equation $Ex_{in,G}$ is the sum of the exergies of all input streams, $Ex_{out,G}$ is the sum of the exergies of all output streams, the index i denotes the i -th component, $W_{rev,i}$ the reversible work (generated or consumed), $Ex_{lost,i}$ the exergy lost or dispersed to the ambient (i.e. the “external losses”) of the i -th component, respectively, Irr_G is the irreversibility due to the exergy destruction rate occurring at a system level (i.e. the “internal losses”).

Irreversibilities can arise from direct dissipation of work (e.g. friction and ohmic resistance) or from spontaneous non-equilibrium processes such as chemical reaction, free diffusion, unrestrained expansion and equalization of temperature, etc.

4.3 Performance exergy indexes and exergy destruction ratio

The performance indexes based on the exergy balance (hydrogen production exergy-based efficiency, heat production exergy-based efficiency, combined hydrogen and heat exergy-based efficiency), are defined as the ratio between the output exergy stream (hydrogen/heat) or their sum and the input exergy stream (biogas, air, water) i.e. $Ex_{in,G}$:

$$\varepsilon_{H_2} = \frac{Ex_{out,H_2}}{Ex_{in,biogas} + Ex_{in,water} + Ex_{in,air}} \quad (8)$$

$$\varepsilon_{Heat} = \frac{Ex_{out,Heat}}{Ex_{in,biogas} + Ex_{in,water} + Ex_{in,air}} \quad (9)$$

$$\varepsilon_{CHH} = \frac{Ex_{out,H_2} + Ex_{out,Heat}}{Ex_{in,biogas} + Ex_{in,water} + Ex_{in,air}} \quad (10)$$

To give a direct causal relationship between component irreversibilities and their effect on the plant exergy efficiency, the *exergy destruction ratio* [9], also known as the *i -th component efficiency defect* [24], is introduced. It represents the part of the overall input exergy destroyed

in the i -th component and can be calculated, including the effect of both the irreversibilities and the external exergy losses, as:

$$\delta_{Irr,i} = \frac{Irr_i + Ex_{lost,i}}{Ex_{in,G}} \quad (11)$$

5. The exergy plant assessment

In this section, the exergy analysis of the two plants will be assessed at system level and component level to provide a deep investigation of the most significant irreversibilities and exergy destruction ratios in the two plants. Moreover, in order to highlight the impact of the single process type on the exergy destruction, a further analysis is carried out by grouping the plant components in different functional areas.

5.1 Exergy analysis results at system level

Figures 4 and 5 show the overall system exergy balance (Grassman Diagram) for the B2H_SR and B2H_ATR plant configurations.

The exergy input (247.3 kW vs 364.9 kW) is mainly due to the exergy of the biogas since the physical exergies of the other input material streams, water and air, are quite negligible (the sum is equal to 2.0 kW), due to their temperature (20°C) close to the reference one. The useful exergy outputs are the hydrogen exergy flux, equal to 146.6 kW for both the configurations and the heat exergy flux, greater in the B2H_ATR plant due to the higher amount of heat available (114.4 kW vs 31.9 kW) as reported in table 4. The external irreversibilities (Ex_{lost}), that summarize the exergy of the effluent streams and all low exergy streams leaving the system without yielding a product (i.e. low temperature flue gas and heat rejected by the coolers to the ambient), is smaller in the B2H_SR plant configuration than in the B2H_ATR one (15.7 kW vs 21.1 kW), even if its percentage with respect to the total exergy input is greater (6.8% vs. 5.8%). Moreover, it is worth noting that the term regarding the reversible work is not reported because it is not an output stream of the plant; in fact, the SOFC power unit is designed and sized to

satisfy only the system energy needs, including the BOP auxiliaries consumption, and not for the electric energy production.

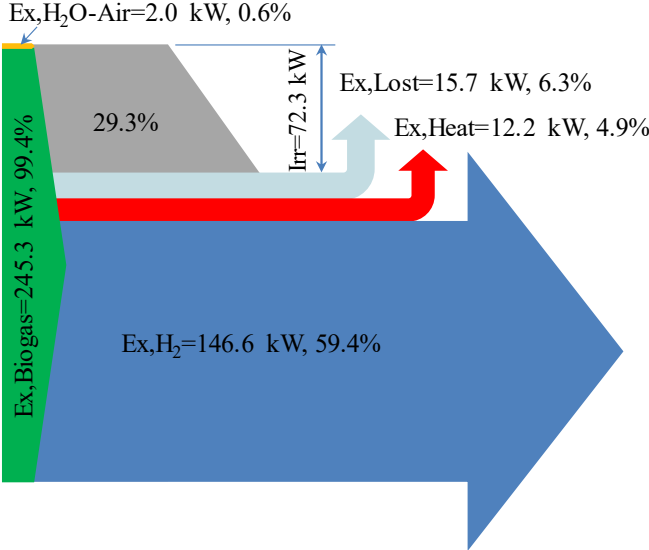


Figure 4. Global Exergy Balance for the B2H_SR plant

Finally, for the B2H_SR the internal irreversibilities destroy the 29.3% (72.3 kW) of the exergy input, while in the B2H_ATR they cause the destroying of the 38.4% (115.8 kW) of the exergy input. Therefore, it can affirm that the quality of the energy conversion in the SR based layout is better than in the ATR one.

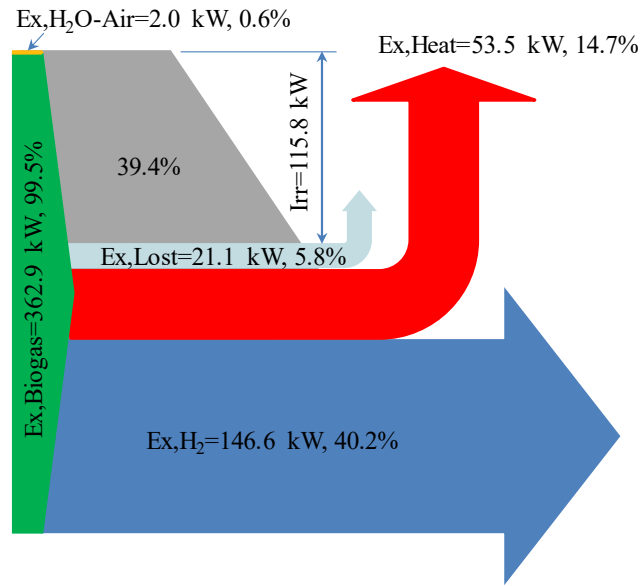


Figure 5. Global Exergy Balance for the B2H_ATR plant

Table 5 presents the performance comparison of the two proposed plant configurations based on the energy balance and the exergy balance.

Table 5. Energy- and Exergy-based Efficiencies comparison for the B2H_SR and B2H_ATR plants

Plant Configuration	B2H_SR		B2H_ATR	
	η (%)	ε (%)	η (%)	ε (%)
Hydrogen production	59.8	59.4	40.4	40.2
Heat production	13.7	4.9	33.6	14.7
Combined Hydrogen and Heat Production	73.5	64.4	73.9	54.8

In the B2H_SR, the biogas conversion is more shifted to the hydrogen production from both the energy and exergy points of view with respect to the B2H_ATR configuration. As a matter of fact, the hydrogen efficiency based on the energy balance is equal to 59.8% vs. 40.4%, while the hydrogen exergy efficiency is equal to 59.4% vs. 40.2%. Regarding the combined hydrogen and heat production, the B2H_ATR layout shows a comparable first law efficiency (73.9% vs. 73.5%) but a lower exergy efficiency (54.8% vs. 64.4%) with respect to the B2H_SR one. Thus, it is worth noting how the exergy analysis approach, by reducing the weight of the heat production, can estimate the quality of the energy conversion process. However, since the aim of this system is to produce hydrogen for mobility applications, the SR layout appears to be more promising.

From the perspective of the hydrogen production for mobility, the B2H_SR layout is in general the preferable choice that allows reducing the biogas consumption of about 32.5%. The heat production at a thermal level of 334°C can be further exploited in the subsequent refrigeration process as requested in the refueling station (-40°C) [25] by adopting an absorption chiller system. However, the B2H_ATR layout, globally more exothermal, could be selected in presence of a local thermal demand that exceeds the refueling station need and that can usefully exploit the high-grade heat (570°C and 405°C) made available by this layout.

5.2 Exergy Analysis results at component level

In order to take into account the exergy dispersed to the ambient by the exhausts (the flue gas generated by the catalytic burner) a flue gas stack is considered as further plant component. Moreover, for this component and for those that do not exchange useful exergy within the system such as the coolers, which reject exergy directly to the environment, the exergy efficiency was not calculated. For the intercooled compressor C1 and the ionic compressor IC, the exergy, due to the heat fluxes discharged to the environment, was included in the irreversibility.

Table 6 reports the exergy balance, at components level, of the B2H_SR plant configuration.

Table 6. B2H_SR Layout: Component Exergy Balance

	$W_{rev,i}$	$Ex_{input,i}$	$Ex_{output,i}$	Irr_i	$Ex_{lost,i}$	ϵ_i	$\delta_{Irr,i}$
	[kW]	[kW]	[kW]	[kW]	[kW]	[%]	[%]
SOFC (DC)	25.00	56.62	28.37	3.25	-	94.25	1.32
DC/AC Conv	-1.00	25.00	24.00	1.00	-	96.00	0.41
CB	-	127.42	86.64	40.79	-	67.99	16.53
SR	-	339.35	333.74	5.61	-	98.35	2.27
WGSR	-	238.21	237.81	0.40	-	99.83	0.16
HE1	-	307.99	299.15	8.84	-	97.13	3.58
HE2	-	27.06	25.54	1.52	-	94.39	0.61
HE3	-	269.39	268.06	1.33	-	99.51	0.54
HE4	-	475.74	475.46	0.27	-	99.94	0.11
C1	-7.00	232.10	236.91	2.20	-	99.08	0.89
C2	-4.00	137.02	140.26	0.76	-	99.46	0.31
IC	-11.00	139.31	146.62	3.69	-	97.55	1.49
Cooler1	-	139.24	137.02	-	2.22	-	0.90
Cooler2	-	140.26	139.31	-	0.95	-	0.38
Cooler3	-	234.42	233.38	-	1.04	-	0.42
Pd-M	-	241.04	237.91	3.13	-	98.70	1.27

SEP	-	233.38	232.29	1.09	-	99.53	0.44
Flue gas Stack	-	8.90	-	-	8.90	-	3.61
Auxiliaries	-2.00	-	-	-	2.00	-	-

In the SR-based layout, the main contributor to the internal exergy losses is the catalytic burner (40.8 kW), with an exergy efficiency of about 68% and an exergy destruction rate of about 16.5%. This low exergy efficiency depends on both the high amount of the combustion air, that increases the mixing irreversibility, and the combustion reactions, that increase the entropy generation.

The second irreversibility source is due to the heat exchange in HE1 because of the water phase changes that involve high temperature gradient above all during the vaporization. In this component, the exergy destruction rate reaches the 3.6% (8.8 kW).

The Steam Reformer reactor has a high exergy efficiency (98.3%) even if a high internal loss, equal to 5.61 kW (2.3% of exergy destruction ratio), can be observed. This is due to the mixing irreversibility (i.e. the mixing between steam and biogas inside) and the heat exchange under finite temperature difference, since the CB exhausts supply the heat for the reforming reaction through a surface heat exchanger.

The further components with high exergy destruction values are the SOFC power unit, the Ionic Compressor and the Pd-Membrane.

Table 7 illustrates the component exergy balance of the B2H_ATR plant configuration. The components that have the lowest exergy efficiencies are the catalytic burner CB and the ATR reactor (74.1% and 88.6%, respectively). In these components, the exergy destruction rates are very high (9.3% and 12.2%, respectively) due to the mixing and combustion irreversibilities.

As in the B2H_SR layout, the heat exchanger HE1, where the water changes phase, shows high irreversibility (18.6 kW) that corresponds to an exergy destruction rate of 5.1%. This value is higher than that calculated in the SR-based configuration because of the largest water flow rate.

The heat exchanger HE4, that is used to preheat air for the ATR reactor, has a high irreversibility

(1.68%) and also the lowest exergy efficiency (93.7%) with respect to the others heat exchangers because of the highest temperature gradients. High values of exergy destruction occur in the Pd-Membrane and in the compressor C1 that elaborates a greater syngas mass flow rate and pressure ratio (152.1 kg/s, 8.0) with respect to the SR-based layout ones (55.3 kg/s, 4.6).

Table 7. ATR-based Layout: Component Exergy Balance

	$W_{rev,i}$	$Ex_{input,i}$	$Ex_{output,i}$	Irr_i	$Ex_{lost,i}$	ϵ_i	$\delta_{Irr,i}$
	[kW]	[kW]	[kW]	[kW]	[kW]	[%]	[%]
SOFC (DC)	38.00	95.29	51.70	5.59	-	94.13	1.53
DC/AC Conv	-1.60	38.00	36.40	1.60	-	95.79	0.44
CB	-	131.48	97.46	34.02	-	74.12	9.33
ATR	-	391.74	347.07	44.67	-	88.60	12.24
WGSR	-	223.25	222.80	0.45	-	99.80	0.12
HE1	-	349.69	331.05	18.64	-	94.67	5.11
HE2	-	65.67	61.76	3.91	-	94.04	1.07
HE3	-	434.70	431.28	3.42	-	99.21	0.94
HE4	-	97.61	91.47	6.13	-	93.72	1.68
HE5	-	304.02	300.45	3.57	-	98.83	0.98
C1	-18.40	209.72	221.75	6.37	-	97.21	1.75
C2	-4.00	137.02	140.26	0.76	-	99.46	0.21
IC	-11.00	139.31	146.62	3.69	-	97.55	1.01
Cooler1	-	139.24	137.02	-	2.22	-	0.61
Cooler2	-	140.26	139.31	-	0.95	-	0.26
Pd-M	-	228.61	218.73	9.89	-	95.68	2.71
SEP	-	212.08	210.99	1.09	-	99.49	0.30
Flue gas Stack	-	14.90	-	-	14.90	-	4.08
Auxiliaries	-3.00	-	-	-	3.00	-	0.82

5.3 Exergy destruction analysis

In order to highlight the impact of every process on the exergy destruction, different functional areas have been defined by grouping the plant components. These functional areas are: i) the Energy Production area, consisting of the SOFC power unit and the DC/AC converter, ii) the Chemical Processing area, grouping the reforming reactor (SR or ATR) and the shifter (WGSR); iii) the Combustion Process area, consisting only of the catalytic burner (CB); iv) the H₂ Separation area, including the syngas compressor (C1), the membrane unit (Pd-M) and the Cooler3 for the SR layout; v) the H₂ Compression area, consisting of the compressor (C2), the

ionic compressor (IC) and the two intercoolers; vi) the Heat Recovery area, including all the heat exchangers.

The exergy destruction is calculated for each functional area by means of eq.5. Figure 6 shows the percentage contribution of the functional areas to the exergy destruction for the two proposed plant configurations.

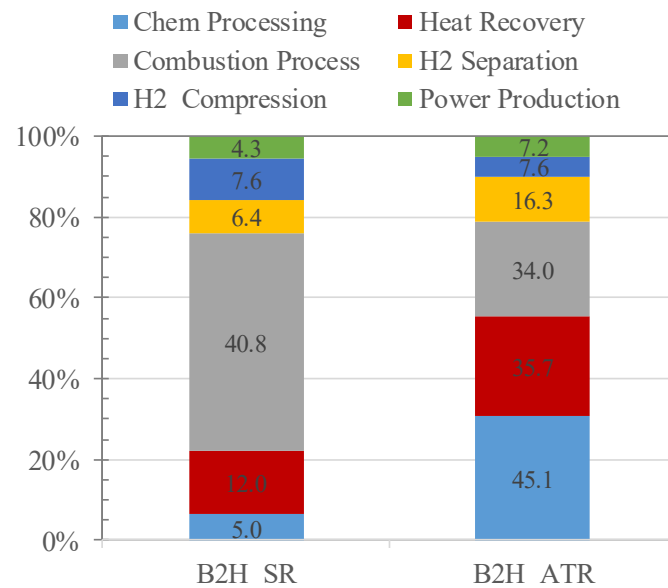


Figure 6. Exergy destruction share by functional area in the plant configurations (labels are the internal irreversibilities expressed in kW)

In the B2H_SR plant, the Combustion Process area is the main contributor (40.8 kW, 54%) to the exergy destruction due to low exergy efficiency, while in the B2H_ATR it causes 34.0 kW (23%) of the exergy destruction rate.

The Chemical Processing area destroys much more exergy in the B2H_ATR (45.1 kW, 31%) than in B2H_SR (5.0 kW, 6.0%), because the heat required to sustain the reforming reactions in the ATR reactor is internally supplied by partial oxidation of an input biogas fraction. The Heat Recovery area contributes to the exergy destruction with 12.0 kW (16%) and 35.7 kW (25.0%) in the B2H_SR and B2H_ATR, respectively, meaning that in the B2H_SR layout the

heat recovery is more optimized with a lower number of heat exchangers, transferring 13.7% less exergy.

The Hydrogen Separation area destroys 6.4 kW (8.0%) in the SR-based layout and 16.3 kW (11%) in the ATR-based layout. As already underlined, these different values are mainly due to the lower flow rate (55.3 kg/h vs 152 kg/h) and the higher hydrogen content (64.0% vs 39.3%) that characterize the syngas in the SR-based configuration. It can be noted that the higher power requested by this functional area has a direct impact on the size of the fuel cell and thus on the related consumption and losses.

The Hydrogen Compression area, operating under the same conditions, requires the same amount of energy and destroys the same amount of exergy, 7.6 kW, representing 10% of the overall losses in the SR-based configuration and 5.0% in the B2H_ATR.

The energy production area destroys about 5.0% of the total exergy losses, in both layouts.

The component that differences in the two layouts is the Coolers 3 that in the SR-based layout discharges 1 kW of exergy to the ambient.

6. Literature comparison

The obtained results have been compared with those available in the scientific literature concerning the green hydrogen production from biogas. The comparison, illustrated in table 8, has been performed considering the adopted technologies and the hydrogen production capacity. With referring to the reforming technologies (SR vs. ATR), the results presented in ref. [1] are congruent with this work results, i.e. better performance, in terms of hydrogen production energy-based efficiency, is obtainable by using the SR process. The comparison between the absolute value of the efficiencies estimated in this work with respect to those presented in ref. [1] highlights that using i) the SOFC technology for the energy supply instead

of an electrical external supplied at the average grid efficiency, ii) the membrane technology for the hydrogen separation instead of PSA technology, iii) the ionic compressor, IC, instead of a more conventional compression technology allows reaching best energy performance (59.8% vs. 46% for SR based system and 40.4% vs. 26% for the ATR based system).

Similarly, the plant configuration (based on the SR technology) proposed in ref. [3], in which an external source is used for the energy supply and the PSA technology is applied for the hydrogen separation, shows a lower efficiency (47%) in comparison to the efficiency calculated in this work (59.8%)

The hydrogen production plant presented in ref. [4] is based on the ATR-MR technology that, by integrating the reforming process with the hydrogen separation (membrane reactor), assures a good performance (57.5%), comparable to that estimated in this work for the B2H_SR plant (59.8%).

The hydrogen production exergy-based efficiency (55%) estimated in ref. [5] is in accordance with the value presented in this work (59.4%), even if the hydrogen compression and storage section is not considered.

Finally, all configurations of the hydrogen production biogas-fed plants presented in ref. [6], by implementing technologies with lower performances (i.e. ICE) and by using the electrolysis process for hydrogen production show worst exergy-based efficiencies.

Table 8. Comparison of results with literature data on biogas to hydrogen conversion systems

Ref.	Technology			H ₂ production and performance data			
	H ₂ production	Power Generation	H ₂ Separation	Flow rate (kg/h)	η_{H_2} (%)	ε_{H_2} (%)	Note
This work	SR	SOFC	Pd-M	4.17	59.8	59.4	820 bar
This work	ATR	SOFC	Pd-M	4.17	40.4	40.2	820 bar
[1]	SR	External	VPSA	4.17	46.0	-	700 bar
[1]	ATR	External	VPSA	4.17	26.0	-	700 bar
[3]	SR	External	PSA	90	47.0	-	10 bar 25°C
[4]	ATR MR	External	MR*	4.17	57.5	-	700 bar

[5]	Dry Reforming	CCGT	PSA	477.8	-	55.0	1.5 bar
[6]	Alkaline EL	ICE	-	24.8	-	19.8	1 bar 80°C
[6]	PEM EL	ICE	-	26.1	-	20.66	1 bar 80°C
[6]	HT EL	ICE	-	36.2	-	25.83	5 bar 800°C

* The Membrane is integrated in the ATR

7. Conclusions

In this study the polygeneration of hydrogen, heat, and electricity is proposed through the designing of two biogas-based plants that differ for the fuel reforming process: the Steam Reforming process, and the Autothermal Reforming process. Four sections define the plants' arrangement: 1) the Reforming Section, 2) the Power Section based on solid oxide fuel cell technology, 3) the Separation Section based on Pd-Ag membrane separation technology, and 4) the Compression and Storage Section using the ionic compression technology.

The hydrogen production plants are studied and compared by applying the energy and exergy analyses.

Results of the energy analysis show that the plant with the Steam Reforming process has a hydrogen production energy-based efficiency higher of about 19 percentage points with respect to that of the configuration based on the Autothermal Reforming. This is due to the better quality of the syngas produced in the reforming section that allows reducing the plant energy consumption (i.e. the power required to bring the syngas up to the operating pressure of the membrane separation unit is lower because of both the smaller syngas flow rate and the pressure ratio). On the contrary, the combined hydrogen and heat energy-based efficiency is almost equal (73.5% vs. 73.9%) since the Autothermal Reforming configuration, thanks to the greater flow rates of the hot streams, makes available, as by-product, a larger quantity of heat for thermal utilities.

A detailed exergy analysis of the two plant configurations has been performed under different points of view (system, component, and functional area level) in order to provide a deep investigation of the most significant irreversibilities and exergy destruction ratio. At the system level, the quality of the energy conversion in the Steam Reforming based layout is confirmed better than in the Autothermal Reforming one. As a matter of fact, the Steam Reforming layout is much more performant regarding the hydrogen production exergy-based efficiency (59.4% vs. 40.2%), as well as the combined hydrogen and heat exergy-based efficiency (64.4% vs. 54.8%).

Moreover, the results of the component level exergy analysis demonstrate that the main contributors to the internal plant irreversibilities are the components where combustion reactions occur. These results are confirmed by the exergy destruction analysis.

Therefore, it can affirm that in the Steam Reforming -based layout, the biogas conversion is more shifted to the hydrogen production from both the energy and exergy points of view in comparison with Autothermal Reforming -based configuration.

Finally, it is possible to note that the advanced technologies adopted in the plant design (i.e. fuel cell, Pd membrane, Ionic Compressor) allow enhancing the energy and exergy efficiencies of more than 10 percentage points with respect to the state of art.

References

1. Di Marcoberardino G, Vitali D, Spinelli F, Binotti M, Manzolini G. Green hydrogen production from raw biogas: A techno-economic investigation of conventional processes using pressure swing adsorption unit. *Processes*. 2018;6(3):19

2. Zeibi Shirejini S, Fattahi M, Mathematical Modeling and Analytical Solution of Two-Phase Flow Transport in an Immobilized-cell Photobioreactor through the Homotopy Perturbation Method (HPM), *Int. J. Hydrogen Energy*. 2016;4:18405-417
3. Yao J, Kraussler M, Benedikt F, Hofbauer H, Techno-economic assessment of hydrogen production based on dual fluidized bed biomass steam gasification, biogas steam reforming, and alkaline water electrolysis processes, *Energy Convers. Manag.* 2017;145:2778-292
4. Di Marcoberardino G, Foresti S, Binotti M, Manzolini G. Potentiality of a biogas membrane reformer for decentralized hydrogen production, *Chemical Engineering & Processing: Process Intensification*.2018;129:131–141
5. Cruz PL, Navas-Anguita Z, Iribarren D, Dufour J, Exergy analysis of hydrogen production via biogas dry reforming, *Int. J. Hydrogen Energy*. 2018;43(26):11688–695.
6. Abusoglu A, Ozahi E, Kutlar AI, Demir S, Exergy analyses of green hydrogen production methods from biogas-based electricity and sewage sludge, *Int. J. Hydrogen Energy*. 2017;42:10986-996.
7. Cohce MK, Dincer I, Rosen MA. Energy and exergy analyses of a biomass-based hydrogen production system. *Int J Hydrogen Energy*. 2011;102:8466-74.
8. Rostamzadeh H, Gargari SG, Namin AS, Ghaebi H. A novel multigeneration system driven by a hybrid biogas-geothermal heat source, Part II: Multi-criteria optimization, *Energy Convers. Manag.* 2019;180:859–888.
9. Dincer I, Zamfirescu C, Renewable-energy-based multigeneration systems, *Int. J. Energy Res.* 2012;36(15):1403-1415.
10. Ahmadi P, Dincer I, Rosen MA, Development and assessment of an integrated biomass-based multi-generation energy system, *Energy*. 2013(56):155-166.
11. Bhattacharya A, Das A, Datta A. Exergy based performance analysis of hydrogen production from rice straw using oxygen blown gasification. *Energy* 2014;69:525-33.

12. Minutillo M, Perna A, Sorce, A. Combined hydrogen, heat and electricity generation via biogas reforming: Energy and economic assessments. *Int J Hydrogen Energy* 2019; 44(43): 23880-98.
13. Di Bona D, Jannelli E, Minutillo M, Perna A, Investigations on the behaviour of 2 kW natural gas fuel processor, *Int J Hydrogen Energy* 2011;36(13):7763-70.
14. Palma V, Ricca A, Ciambelli P. Fuel cell feed system based on H₂ production by a compact multi-fuel catalytic ATR reactor. *Int J Hydrogen Energy*. 2013;38:406-16.
15. Montenegro Camacho YS, Bensaïd S, Lorentzou S, Vlachos N, Pantoleontos G, Konstandopoulos A, et al. Development of a robust and efficient biogas processor for hydrogen production. Part 1: Modelling and simulation. *Int J Hydrogen Energy*.2017;42:22841-55.
16. Araki S, Hino N, Mori T, Hikazudani S, Autothermal reforming of biogas over a monolithic catalyst, *Journal of Natural Gas Chemistry*. 2010;19:477–481.
17. Rau F, Herrmann A, Krause H, Fino D, Trimis D, Production of hydrogen by autothermal reforming of biogas, *Energy Procedia*, 2017; 120:294-301.
18. Perna A, Minutillo M, Jannelli E, Cigolotti V, Nam SW, Sung PY. Performance assessment of a hybrid SOFC/MGT cogeneration power plant fed by syngas from a biomass down-draft gasifier. *Applied Energy*. 2018;227: 80-91.
19. Perna A, Minutillo M, Jannelli E, Cigolotti V, Nam SW, Han J. Design and performance assessment of a combined heat, hydrogen and power (CHHP) system based on ammonia-fueled SOFC, *Applied Energy*. 2018;231: 1216-1229
20. Bejan A, Tsatsaronis G, Moran M. (1996). *Thermal Design and Optimization*. John Wiley & Sons, Inc., New York.
21. Terzi R. *Application of Exergy Analysis to Energy Systems*. *Application of Exergy*, 2018, 109, Interchopen.

22. Sciubbia E, Wall G, A brief commented history of exergy from the beginnings to 2004, *Int. J. Thermodyn.* 2007;10 (1):1-26.
23. Todd B, Young JB. Thermodynamic and transport properties of gases for use in solid oxide fuel cell modelling. *J. Power Sources.* 2002;110:186–200.
24. Kotas TJ, *The exergy Method of Thermal Plant Analysis* Exergon Publishing Company UKLtd, London (2012).
25. Reddi K, Elgowainy A, Rustagi N, Gupta E. Impact of hydrogen SAE J2601 fueling methods on fueling time of light-duty fuel cell electric vehicles, *Int J Hydrogen Energy.* 2017;42:16675-685.
26. Gallucci F, Medrano J, Fernandez E, Melendez J, van Sint Annaland M, Pacheco A. Advances on High Temperature Pd-Based Membranes and Membrane Reactors for Hydrogen Purification and Production. *Journal of Membrane Science and Research* 2017;3(3):142-156
27. <https://www.hysep.com/fileadmin/hysep/user/documents/B-09-010-Module-1308.pdf>
28. Linde. Hydrogen technologies. The Ionic Compressor 90 MPa – IC90. Technical brochure; 2015
29. Linde. Linde’s innovative technologies for the hydrogen infrastructure. 2015
30. Mayer M. From prototype to serial production: Manufacturing hydrogen fuelling stations. A3PS Ecomobility Conference, 20 October 2014, Vienna, Austria.
31. Aspen Plus Software, V8.8, <https://www.aspentech.com>
32. Perna A, Cicconardi SP, Cozzolino R. Performance evaluation of a fuel processing system based on membrane reactors technology integrated with a PEMFC stack, *Int J Hydrogen Energy* 2011;36(16):9906-15.

Appendix A

In this Appendix, the flowsheets of the thermochemical and electrochemical models of the proposed plant configurations are reported and briefly described. Moreover, some details on the models validation, widely described in the cited references, are illustrated. The data used for the validation processes are obtained from experimental activities [13,18] or derived from product sheets declared by manufacturers [26-30].

A1. Integrated models flowsheets

Figures A1 and A2 show the flowsheets of B2H_SR and B2H_ATR models realized in Aspen Plus™ environment [31]. The integrated models of the plants have been developed by using existing unit operation blocks and user defined blocks (i.e. Hierarchy block) with a modular approach.

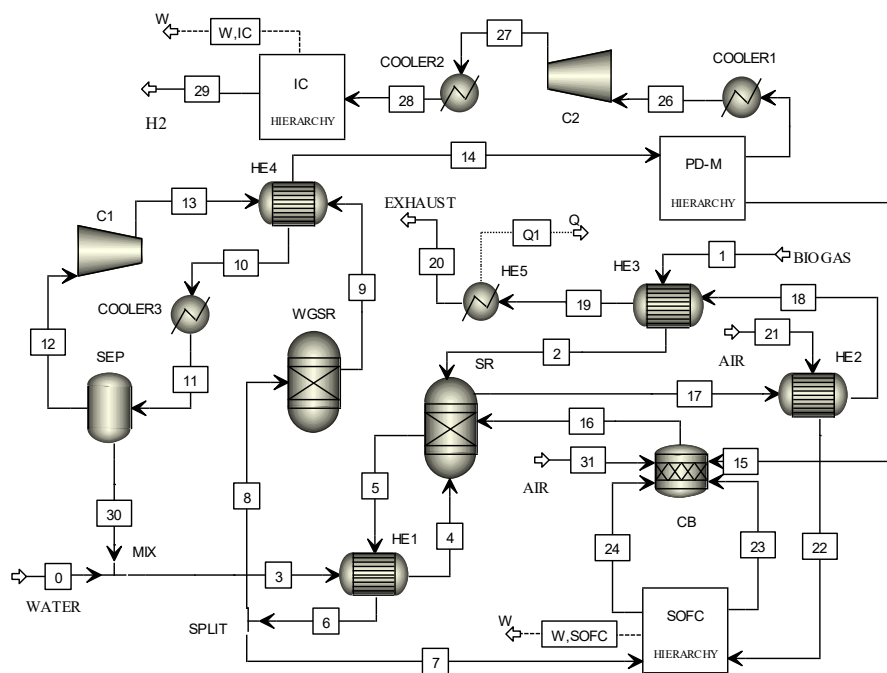


Figure A1. Flowsheet of the B2H_SR model

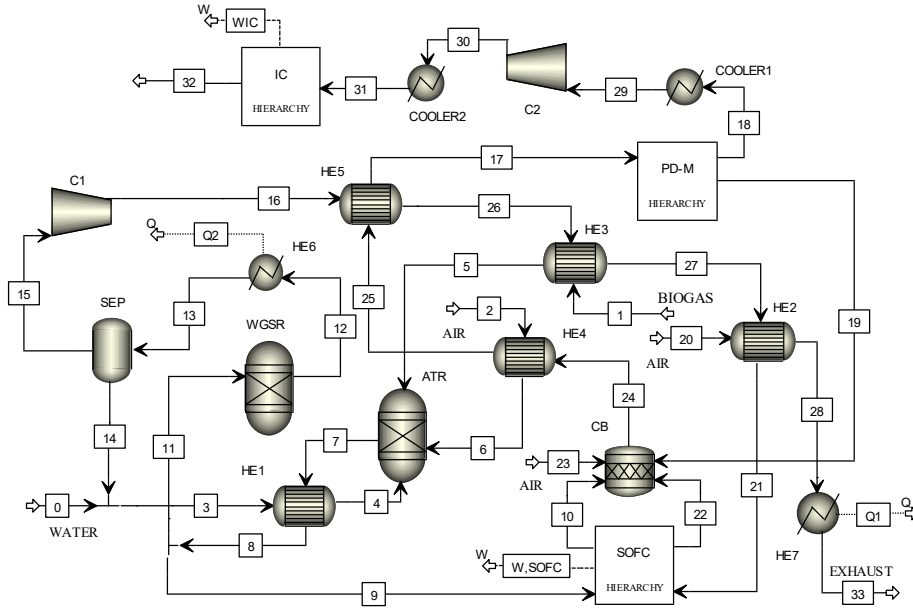





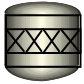

Figure A2. Flowsheet of the B2H_ATR model

Table A1 summarized the main characteristics of the thermochemical and electrochemical models used for simulating each component of the proposed plant configurations. For SOFC, and Pd-M, user defined blocks have been built by means of unit operation blocks and Fortran calculator blocks.

Table A1. Details on the numerical models developed for the plants simulations.

Plant Components	Sub-model description
Reforming reactors (SR and ATR) and Water Gas Shift reactors (WGSRs) 	The reformers and the shifters are modeled by using the <i>RGibbs</i> unit operator block where no reaction kinetics are applied. The <i>RGibbs</i> uses the Gibbs free energy minimization to calculate the equilibrium and does not require specified reaction stoichiometry. The Gibbs free energy of the reaction system (k species) is: $G^t = \sum_{i=1}^k n_i \cdot \mu_i \quad A1$ where n_i is the moles number of species i , and μ_i is its chemical potential. For the WGSRs, the methane eventually present in the reactant flow is considered as an inert.
SOFC unit (SOFC)	By starting from a cell-level approach widely discussed and detailed in previous papers [18,19], the SOFC unit model is built for predicting the stack behavior and performance in terms of polarization curves under different working conditions such as temperature, pressure and anode and cathode gasses composition. The mass and energy balances as well as the output streams composition are calculated by considering not only the electrochemical reactions which occur on the anode and cathode catalysts but also the

<div style="border: 1px solid black; padding: 5px; width: fit-content; margin: auto;"> SOFC HIERARCHY </div>	<p>thermo-chemical reactions (steam reforming and water gas shift) that can take place in the anode side because of the high operating temperatures and the composition of the feeding fuel. The elemental cell is modeled through unit operation blocks (<i>RStoich</i> and <i>RGibbs</i> for the anode, <i>Sep</i> for the cathode, thermal mixer and splitter for the thermal balance), and a Fortran block calculator in which the electrochemical relations (overvoltage losses, voltage, current, etc) for the cell behavior prediction are implemented, as described in [18].</p> <p>The stack voltage (the average cell stack voltage) is calculated by means of the cell area-specific resistance (ASR_{cell}) and the stack loss factor (the ratio between the stack area-specific resistance and the cell area-specific resistance) [18]:</p> $V_{stack} = f_{stack} \cdot ASR_{cell} \cdot \frac{I}{A_{cell}} \cdot n_{cell} \quad A2$ <p>The cell area specific resistance is:</p> $ASR_{cell} = \frac{\eta_{act,cat} + \eta_{act,an} + \eta_{ohmic} + \eta_{con,an} + \eta_{con,cat}}{I} \cdot A_{cell} \quad A3$ <p>where $\eta_{act,an}$ and $\eta_{act,cat}$ are the anodic and cathodic activation overpotentials, η_{ohmic} is the ohmic overpotential, $\eta_{con,an}$ and $\eta_{con,an}$ are the anodic and cathodic concentration overpotential due to mass transfer limitations.</p> <p>The stack electric power is:</p> $W_{stack} = V_{stack} \cdot I \cdot n_{cell} \quad A4$
<p>Pd-Membrane (Pd-M)</p> <div style="border: 1px solid black; padding: 5px; width: fit-content; margin: auto;"> PD-M HIERARCHY </div>	<p>The parameters that drive the hydrogen permeation through the membrane are its concentration in the feeding gas, the operating temperature and the pressure gradient between the feed and permeate sides.</p> <p>The equations used to simulate the permeation process are reported in [19, 32]. The inputs to the model are the hydrogen recovery ratio (HRF) that is the ratio between the permeate hydrogen (mol/s) and the hydrogen (mol/s) in the feed stream, the feed and permeate sides pressures, the membrane thickness and operating temperature. The outputs are the membrane total area, the amount of permeate hydrogen (mol/s) and the retentate gas flow rate (mol/s) and composition.</p> <p>The flow rate of the total permeated hydrogen (mol s⁻¹) is:</p> $n_{H_2,perm} = J_{H_2,perm} \cdot A_{perm} = N_m N_t \cdot A_{perm,tube} \quad A5$ <p>where $J_{H_2,perm}$ is the hydrogen permeation flux [19], A_{perm} (m²) is the permeation area, $A_{perm,tube}$ is the single tube permeation area, N_m the modules number and N_t the number of tubes in each module. The Pd-Membrane unit is modeled by means of a separator block and a Fortran block calculator in which the model equations are implemented.</p>
<p>Ionic Compressor (IC)</p> <div style="border: 1px solid black; padding: 5px; width: fit-content; margin: auto;"> IC HIERARCHY </div>	<p>The ionic compressor works at near isothermal conditions. In order to simulate these conditions, the compression is carried out by means of 5 stages, each of which consists of an adiabatic compressor and a heat exchanger where the heat removed is the 90% of the work consumed during the adiabatic compression [19]. The compressor power of each stage is calculated as:</p> $W_i = \dot{m}_{H_2} \cdot c_{p,H_2} \cdot T_{in,i} \cdot \left[\left(\frac{p_{out,i}}{p_{in,i}} \right)^{\frac{k-1}{k} \frac{1}{\eta_{pol}}} - 1 \right] \quad A6$ <p>where the k is the ratio of the specific heats, c_{p,H_2} is the hydrogen specific heat at constant pressure, $T_{in,i}$ (K), $p_{in,i}$ and $p_{out,i}$ are the inlet temperature the inlet pressure and outlet pressure at each stage (i) respectively and η_{pol} is the polytropic efficiency, assumed equal to 91%.</p> <p>The inlet temperature at each stage is:</p> $T_{in,i} = T_{out,i-1} - \frac{0.9 \cdot W_{i-1}}{\dot{m}_{H_2} \cdot c_{p,H_2}} \quad A7$ <p>The ionic compression power consumption is:</p> $W_{IC} = \sum_i W_i \quad A8$

<p>Heat exchangers (HXs)</p> 	<p>The heat exchangers are modeled by using the HeatX that can perform shortcut or detailed rating calculations for most types of two-stream heat exchangers. For a two-stream exchanger the set of equations are:</p> $Q = \dot{m}_{cold} \cdot \Delta h_{cold} \quad A9$ $Q = \dot{m}_{hot} \cdot \Delta h_{hot} \quad A10$ $Q = U \cdot A \cdot LMTD \quad A11$ <p>where U (kW/m² K) is the heat transfer coefficient, A (m²) is the heat exchange area and LMTD is the log-mean temperature difference.</p>
<p>Compressor (C)</p> 	<p>This component is modeled by using the Compr unit operator block; the compression work is calculated once the outlet pressure or the compression ratio and the isentropic or polytropic efficiency are defined. The compression power is:</p> $W_C = \dot{m}_{stream} \cdot c_{p,stream} \cdot T_{in} \cdot \left[\left(\frac{p_{out}}{p_{in}} \right)^{\frac{k-1}{k} \frac{1}{\eta_{pol}}} - 1 \right] \quad A12$ <p>where the k is the specific heats ratio of the gaseous stream, $c_{p,stream}$ is the specific heat at constant pressure, T_{in} (K), p_{in} and p_{out} are the inlet temperature, the inlet pressure and outlet pressure, respectively, and η_{pol} is the polytropic efficiency.</p>
<p>Catalytic burner</p> 	<p>This component is modeled by means of RStoic that is a reactor in which the stoichiometry is known. The combustion reactions are:</p> $CO + 0.5O_2 \rightarrow CO_2$ $CH_4 + 2O_2 \rightarrow 2H_2O + CO_2$ $H_2 + 0.5O_2 \rightarrow H_2O$
<p>Cooler</p> 	<p>This component allows to simulate a simple heat exchanger in which the outlet temperature or the exchanged heat can be assigned.</p> $Q = \dot{m} \cdot (T_{out} - T_{in}) \quad A13$

A2. Models validation

The models of the reforming and shifting reactors, based on the chemical equilibrium calculated by the minimization of the Gibbs free energy, were validated by using the experimental data measured in a test station designed and realized at the Fuel Cells Lab of the Cassino University [13].

In the test station, the natural gas was used as feeding fuel. Fuel and water (the steam to carbon ratio was 2.5) were converted in a hydrogen rich stream by means of two reactors: a high temperature reactor where the steam reforming took place and a low temperature reactor in which the water gas shift reaction occurred.

Table A2 shows the comparison between the main measured data and the numerical results.

Table A2. Reforming model validation: experimental and calculated data

Data	Measured	Model
Steam Reforming reactor temperature (°C)	670 ± 4	750
Water Gas Shift reactor temperature (°C)	265 ± 10	250
Syngas composition (% vol)		
H ₂	78.30 ± 0.4	77.35
CO ₂	17.80 ± 0.2	18.91
CH ₄	3.60 ± 0.5	3.17
CO	0.64 ± 0.06	0.6

By analyzing the results illustrated in table A1, it can be observed that the assumption of the chemical equilibrium in the reforming processes allows to predict the reactors operating conditions with a good agreement with respect to the measured data.

The calibration and validation of the SOFC model have been performed by means of experimental tests on an anode-supported planar cell (effective area 16 cm²) manufactured by the Korea Institute of Science and Technology (KIST), as detailed in ref. [18]. The tests were carried out under different cell temperature, hydrogen utilization factor, anode gas composition (pure hydrogen or mixtures consisting of H₂, CO, CO₂, N₂ to simulate a syngas).

In table A3 the comparison between the measured and calculated data is illustrated. Results refer to a single cell operation at an operating temperature of 800°C and with an anode feeding gas composition of 12.8 vol% H₂, 15.5 vol % CO, 2 vol% CH₄, 9.78 vol% CO₂, 39.9 vol% N₂, 20 vol% H₂O.

Table A3. SOFC model validation: experimental and calculated data

	Measured	Model	Measured	Model
Current density (A/cm ²)	0.5	0.5	1	1
Voltage (V)	0.821	0.821	0.652	0.709
Anode off-gas (% vol)				
H ₂	18.2%	18.3%	12.9%	12.2%
CO	13.8%	13.1%	10.8%	8.7%
CH ₄	0.25%	0.2%	0.28%	0.2%
CO ₂	18.3%	20.0%	23.1%	26.8%
N ₂	49.5%	48.4%	52.8%	52.1%

As it is worth noting, a good accordance was achieved. Further comparisons in terms of polarization curves gave the same good agreements, as detailed in ref. [18]. The validation

results highlighted that the maximum prediction error in the cell voltage, estimated by using the mean absolute percentage error, was 2.3%.

The Pd-Membrane unit is based on multi-tube modules consisting of supported ceramic Pd-Ag membrane tubes like to the pre-commercial Hysep modules manufactured by the ECN Research Centre [26,27]. Therefore, the validation of the membrane separation model has been carried out by using the technical data of the largest Hysep module, the Hysep 1308 that consists of 13 tubes. By assuming as operating conditions a feed side pressure of 25 bar, a permeate side pressure of 4 bar and a temperature of 390 °C, the membrane total area and the hydrogen permeation flux were calculated. Table A4 summarizes the main operational data and the corresponding model values. Therefore, it can affirm that the membrane model allows a good prediction of the hydrogen permeation process.

Table A4. Membrane model validation: operational and calculated data

Operational data	ECN module Hysep 1308	Model
Hydrogen concentration in the feeding stream (%)	33	33
Membrane thickness (μm)	3-9	9
Tube length (m)	1-1.2	1
Membrane total area (m ²)	0.5	0.52
Hydrogen permeation flux (Nm ³ /h)	3.5-6.0	6.0

The hydrogen compression is realized by adopting the advanced technology of the ionic compression (IC50 and IC90 compressors) proposed and manufactured by Linde Group [28-30]. Figure A4 shows the flowsheet of the IC model.

In table A5 the comparison between the operational data of the IC90 and the calculated values are reported.

Table A5. Ionic Compressor model validation: operational and calculated data

Operational Data	IC90	Model
Hydrogen inlet pressure (bar)	5-200	5
Hydrogen outlet pressure (bar)	900	900
Compression type	Isothermal	Intercooled

Compression stages	5	5
Polytropic efficiency	-	0.91
Heat removed by stage (%)	-	90
Energy requirement (kWh/kg)	2.7	2.68

Thus, the model assumptions (intercooled stage with a polytropic efficiency of 0.91 and a removed heat percentage of 90%) allow calculating the energy requirements accurately.